Laser-induced thermal detachment of hot, large molecular ions under multiphoton-absorption conditions

M. Goto,* J. Matsumoto, H. Shiromaru, and Y. Achiba
Department of Chemistry, Tokyo Metropolitan University, Hachioji, Tokyo 192-0397, Japan

T. Majima† and H. Tanuma
Department of Physics, Tokyo Metropolitan University, Hachioji, Tokyo 192-0397, Japan

T. Azuma
Atomic, Molecular, and Optical Physics Laboratory, RIKEN, Wako, Saitama 351-0198, Japan
and Department of Physics, Tokyo Metropolitan University, Hachioji, Tokyo 192-0397, Japan
(Received 16 November 2012; published 5 March 2013)

We observed the delayed electron detachment induced by multiphoton absorption of hot, zinc phthalocyanine negative ions ($C_{32}H_{16}N_8Zn^-$) stored in an electrostatic ion storage ring. To examine the critical parameters and conditions that characterize the delayed processes, we performed a theoretical model simulation employing inferred values for molecular properties and experimentally controlled values of excitation laser energy and fluence. The thermal detachment rate was estimated by applying the detailed balance theory, and the internal energy distribution of the ions after multiphoton absorption was calculated as a function of the ion temperature immediately before laser irradiation. Our model simulation well reproduces the experimental results, and demonstrates that the experimental configuration determines the range of the observed detachment rate, namely the detectable energy window of the stored ions. The parameter dependence of the estimated ion temperature on the molecular properties was also obtained.

DOI: 10.1103/PhysRevA.87.033406 PACS number(s): 33.80.Eh, 36.20.−r

I. INTRODUCTION

The delayed reaction of isolated molecular ions in vacuum has attracted considerable attention because the reaction is a statistical process inherent to many-body systems, and it has been especially studied for many neutral and ionic species [1]. One of the important conclusions is that the rates of photoinduced delayed reactions are governed by the *sum* of the internal energy before photoabsorption (initial internal energy, $E_{\rm ini}$) and the absorbed photon energy regardless of the individual amount [2]. Because the absorbed energies are experimentally controlled or derived, $E_{\rm ini}$ can be estimated by analyzing the delayed processes.

Electrostatic ion-beam storage devices, such as a linear trap [3–5] and a storage ring [6–9], are suitable for investigating such slow decay processes. These devices have no mass restriction of stored ions, and they allow the observation of reactions through the detection of fast neutral products of approximately ten microseconds to seconds, which are time scales that cannot be accessed using a standard time-of-flight tube. For example, statistical and nonstatistical laser-induced decays of various clusters and biomolecules stored in the electrostatic ion storage ring named ELISA [6] were investigated extensively [10,11]. In the present study, we report the laser-induced delayed detachment of hot macrocyclic molecules after multiphoton absorption measured with an electrostatic ion storage ring, and discuss the observed behavior with the aid of model simulations.

Laser-induced statistical decay is typically studied by measuring the intensity of neutral products [$I(t)$] as a function of the time beyond laser irradiation (t). In general, such a decay profile is expressed by the following formula:

$$I(t) \propto \int g(E)k(E)\exp[-k(E)t]dE, \qquad (1)$$

where $g(E)$ is the internal energy distribution after the photoabsorption process and $k(E)$ is the rate constant of the delayed reactions [12–16]. With the exception of the delta-function-like $g(E)$, nonexponential $I(t)$ is expected because of the strong energy dependence of $k(E)$. When $g(E)$ is considerably broad and can be approximated as flat, $I(t)$ follows the $1/t$ decay law [12], and the importance of the nonflat $g(E)$ has been also pointed out [16]. The following propensity rules should be considered for better observation of laser-induced delayed detachment processes. First, the effective temperature after photoexcitation should be high enough to efficiently induce delayed detachment, as is easily understood by Eq. (1). Second, the photon energy is preferably lower than the detachment threshold of the molecular ion; otherwise the direct detachment, which competes with the delayed detachment, dominates [17].

Several groups have analyzed nonexponential $I(t)$ that resulted from *single*-photon detachment processes. On the basis of Eq. (1) Toker *et al*. determined the initial (immediately before photoabsorption) temperature $T_{\rm ini}$ of Al_4^- to be in the range from room temperature to 1400 K [14]. The targets were heated to sufficiently high temperatures using single-photon absorption because of their small heat capacities, even when

*Corresponding author: motoshi-goto@riken.jp; Present address: Atomic, Molecular, and Optical Physics Laboratory, RIKEN.
†Present address: Department of Nuclear Engineering, Kyoto University.

they were initially at room temperature. For large molecules, the excess energy should be considerably high because of their large heat capacities; thus, an alternative approach was adopted. For example, Sundén *et al.* determined the cooling rate of C_{60}^- at temperatures sufficiently high to give rise to significant spontaneous decay before photoabsorption [18].

However, when the target is a large molecular ion at *moderately hot* temperatures, these single-photon methods are difficult to apply because of the restrictions mentioned above. Thus, *multiple*-photon processes are required to sufficiently heat such a molecular ion, even a more complicated analysis is needed.

In a previous study, we reported multiphoton-induced delayed detachment of hot zinc phthalocyanine negative ions ($C_{32}H_{16}N_8Zn$, hereafter $ZnPc^-$) stored in an electrostatic storage ring at Tokyo Metropolitan University [19]. The relation of the integrated $I(t)$ over a limited time range (20–1020 μs) against the laser fluence F was well fitted by power functions of F, namely F^b. We ascribed this behavior to the radiative cooling of the ions.

The aim of the present study is to understand the detachment behavior of stored large molecular ions in detail with the aid of model simulation of the decay profiles, $I(t)$, and the integrated intensity, $I_{\rm sum}$, from multiphoton absorption. Through the model simulation, we confirmed the critical concept of "energy window" of the excitation energy of the ions, determined by observing the time range restricted by the experimental configuration. We experimentally observed the delayed detachment process with the corresponding range of the decay constants. In other words, the detection of neutral products after photoexcitation requires the ions to possess an appropriate internal energy. The determining factor in the delayed detachment behavior is the shape of $g(E)$ in Eq. (1) located in the energy window.

In the following discussion, Sec. II describes the relevant experimental setup and configuration, which are critical for the "energy window." Then we present some important experimental observations. Section III explains the simulation procedure and results. We show how our simulation results explain the characteristic detachment behavior and demonstrate the importance of the energy window. Our goal is to estimate the ion temperature, $T_{\rm ini}$, from observations. The estimated $T_{\rm ini}$ strongly depends on the input parameters for which accurate values are not available. Thus, we discuss the parametric dependence of $T_{\rm ini}$ on the molecular properties.

II. EXPERIMENT AND RESULTS

A brief description of the relevant experiments, the data analysis procedure, and typical results are given in this section. More details of the experiments are described in Ref. [19]. A schematic view of the experimental setup is shown in Fig. 1(a). A 15-keV $ZnPc^-$ beam produced in a laser desorption source without any cooling gas was stored in the ring with a revolution time of 110 μs. After a given storage time, the ions were excited with a nanosecond laser pulse on one side of the straight section of the ring. The photon energy of the laser was 1.9 eV (640 nm), which corresponds to the π^*-π^* absorption band [19]. The laser fluence was tuned with neutral-density filters, and was measured during data accumulation by sampling 10%

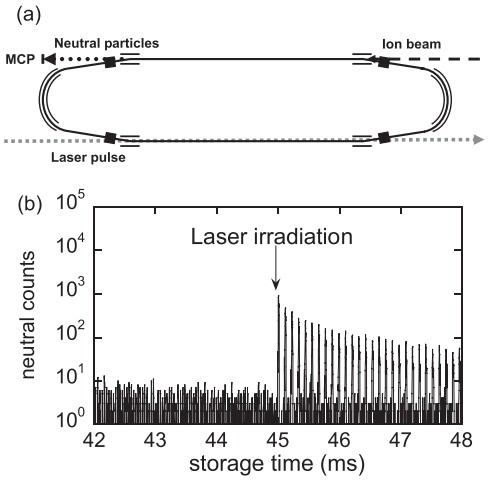

FIG. 1. (a) Schematic view of the experimental setup of an electrostatic ion storage ring at Tokyo Metropolitan University (TMU E-ring). MCP indicates a pair of microchannel plates for detecting the neutral products formed from the decay of the stored ions. (b) A typical time spectrum of the neutral product yield with a logarithmic scale for a storage time from 42 to 48 ms. The stored ions were irradiated by a nanosecond laser pulse after 44.95 ms of storage.

of the pulse separated with a beam splitter. The detector for the neutral products formed by the decay of the stored ions was located at the end of the other straight section opposite to the laser irradiation area. This experimental configuration restricted the time range for detecting the neutral products that resulted from the laser excitation; they could not be detected up to a few tens of microseconds after the irradiation, since the excited ions have to survive at least during the time span for traveling to the other straight section. As will be discussed later, this determines the cutoff of the energy window on the high-energy side.

Figure 1(b) shows an example of the time spectrum of the neutral yields. The enhanced peak appears every 110 μs after the first peak because the heated ions are passed through the straight section for neutral detection turn by turn. The background signal is because of the collisional detachment with residual gas and autodetachment. To derive the enhanced signal in the spectrum, a scaled reference spectrum, which was measured without laser shooting, was subtracted. Integration of each peak and the plot of it against time after the irradiation gives $I(t)$. The yield, $I_{\rm sum}$, is calculated from the sum of the first ten points of $I(t)$. To cancel out the ion-density fluctuation, we normalized it by the sum of the neutral signals in the range from 5 to 20 ms prior to laser irradiation, which is considered to be proportional to the number of stored ions.

Typical experimental results are summarized in Fig. 2. $I(t)$ measured at different storage times with similar laser fluence F (about 4.0 mJ/cm^2) are displayed in Fig. 2(a). A notable feature is that the observed decay curves are not sensitive to storage times. For the hot ions undergoing radiative cooling, storage time is directly related to $T_{\rm ini}$. Thus, the $T_{\rm ini}$-insensitive result is at first puzzling when we naively consider that $I(t)$ curves decay faster for high $T_{\rm ini}$. Although one might interpret that this is the result of very slow radiative cooling, the simulation gives an alternative interpretation, as will be shown later.

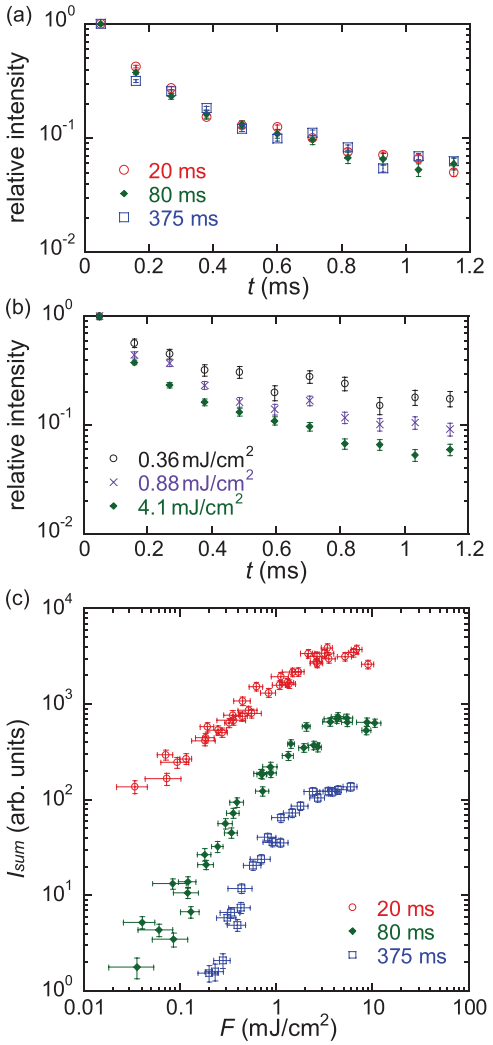

FIG. 2. (Color online) (a) $I(t)$, normalized to the first points, for storage times of 20, 80, and 375 ms. F was 4.1, 4.1, and 3.9 mJ/cm^2, respectively. To increase statistics, three curves were summed and the average F values are indicated. The uncertainties are statistical 1σ values. (b) $I(t)$ for F of 0.36, 0.88, and 4.1 mJ/cm^2, indicated in the same manner as (a). The storage time was 80 ms. The curve for $F = 4.1$ mJ/cm^2 is the same as that for the storage time of 80 ms shown in (a). (c) $I_{\rm sum}$-F plot for the three storage times used in (a). The data for different storage times are shifted for display purposes. The vertical uncertainties are statistical 1σ values combined with the systematic error described in the text, and the horizontal error bars indicate the fluctuation of F.

Figure 2(b) shows the $I(t)$ measured with different F at a storage time of 80 ms, where the $I(t)$ decreases more rapidly against t for higher F. Figure 2(c) shows the F dependence of $I_{\rm sum}$ for the same storage times as those in Fig. 2(a). In the low-F region, a linear relationship in log scale was observed for the each storage time. The slopes become steeper as the storage time increases, agreeing well with the previous results [19]. In the high-F region, beyond the range examined in the previous study, the slope gradually decreases with an increase of F, which is phenomenologically similar to the effect called "saturation" that can be generally observed in action spectra when the excitation is excessively strong.

III. SIMULATION

In this section, we will discuss the simulation procedure concerning the $T_{\rm ini}$ dependence of $I(t)$, the F dependence of $I(t)$, and the F dependence of $I_{\rm sum}$, as shown in Figs. 2(a)–2(c), respectively.

A. Simulation procedure

The simulation procedure is summarized in the following six steps:

Step 1. The energy distribution immediately before photoabsorption, $g_{\rm ini}(E)$, is calculated for a given $T_{\rm ini}$.

Step 2. The energy distribution immediately after photoabsorption, $g(E)$, is calculated from $g_{\rm ini}(E)$ for a given F.

Step 3. $k(E)$ is calculated on the basis of the detailed balance theory [13].

Step 4. From $g(E)$ and $k(E)$, the decay profile $I(t)$ is simulated.

Step 5. $I(t)$ was simulated for various F.

Step 6. $I_{\rm sum}$ was calculated for various F.

We made two assumptions for calculating $g(E)$. The first was that $g_{\rm ini}(E)$ was described in terms of a canonical ensemble of the ions at an effective temperature $T_{\rm ini}$. Then, $g_{\rm ini}(E)$ was calculated from the Boltzmann distribution,

$$g_{\rm ini}(E) = \rho \exp(-E/k_B T_{\rm ini}), \tag{2}$$

where ρ is the density of the vibrational states obtained by counting up the number of states for the neutral molecule [20], and k_B is the Boltzmann constant.

The second assumption concerns the photoabsorption probability of each n-photon process, P_n. It is known that multiphoton absorption gives rise to delayed detachment, provided that the absorbed photon energy is immediately redistributed to the vibrational modes before the next photon is absorbed. This relaxation mechanism explains the delayed detachment of clusters excited with a nanosecond laser pulse [2,21]; therefore, it can also likely describe the delayed detachment of other large molecules. We derived P_n from the Poisson distribution as a function of the average number of photons absorbed by the system, which is considered to be an adequate approximation in earlier studies [22–25],

$$P_n = (\sigma D)^n \exp(-\sigma D)/n!. \tag{3}$$

Here, σ is the photoabsorption cross section, and D is the number of photons per single laser shot passing through the unit-merging area, calculated from F per laser shot and one-photon energy ($h\nu$) using the relation $F = Dh\nu$.

These assumptions lead to the energy distribution after n-photon absorption, $g_n(E)$, expressed as

$$g_n(E) = P_n g_{\rm ini}(E - nh\nu). \tag{4}$$

Finally, $g(E)$ was obtained by

$$g(E) = \sum_n g_n(E), \tag{5}$$

summing all $g_n(E)$ over various n-photon processes, with the exception of $n = 0$, which gives the background signals.

To match the experiments $h\nu = 1.9$ eV was adopted, and F ranged from 0.04 to 10 mJ/cm^2, comparable with that used in the experiments shown in Fig. 2(c). In the present simulation,

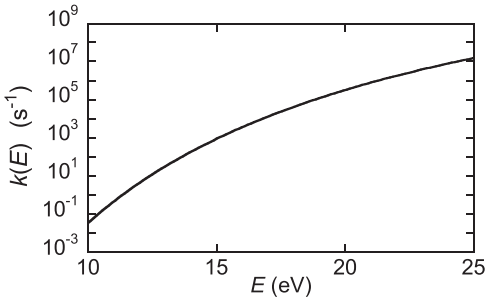

FIG. 3. Plot of the calculated $k(E)$ against E using E_a of 3.3 eV.

we tentatively adopted 2.9×10^{-16} cm^2 for 1.9-eV photons σ, evaluated from the absorption spectra of the ion in solution at room temperature [26].

The detailed balance theory was applied to obtain $k(E)$ [13]. We used the electron attachment cross section of the neutrals of 100 Å^2 calculated from the geometric structure, and a heat capacity of 1.2×10^{-2} eV/K for >900 K estimated from the frequencies of the vibrational modes [20]. To our knowledge, the electron affinity E_a has not been experimentally determined to date, and a theoretical report showed two different values, 3.3 and 3.8 eV, depending on the calculation levels [27]. In the present simulation, we tentatively adopted the value of 3.3 eV, obtained with the higher-level calculation. The $k(E)$ calculated as a function of E is displayed in Fig. 3.

The numerical calculation of $I(t)$ used the following equation with the discrete internal energy component E_j in place of Eq. (1),

$$I(t) = \sum_j g(E_j)k(E_j)\exp[-k(E_j)t]\Delta E_j, \qquad (6)$$

numerically summing up the decay profiles for discrete E_j components after the photoabsorption processes. We calculated $I_{\rm sum}$ by integrating $I(t)$ from Eq. (6) over 50–1050 μs, corresponding to the time region of ten revolutions of the stored ions.

B. Simulation results and discussion

We first describe the general tendency of the simulation results, and then proceed to the discussion of the energy window.

1. *I(t) curves measured with fixed F*

Figure 4 shows $g_{\rm ini}(E)$, $g_n(E)$, and $g(E)$ calculated for three different $T_{\rm ini}$ under the condition of $\sigma D = 4.0$, corresponding to $F = 4.1$ mJ/cm^2 in our experiments and shown in Fig. 2(a). The simulation indicates that various multiphoton processes contribute to $g(E)$ under this fluence condition, making $g(E)$ fairly broad. The $T_{\rm ini}$ dependence apparent in the $g_{\rm ini}(E)$ width becomes less prominent in $g(E)$ because of the strong broadening effect of multiple components, and practically it only leads to a shift in $g(E)$.

This broad feature of $g(E)$ results in the nonexponential time dependence of the calculated $I(t)$, as shown in Fig. 5(a), where the summation is from $E_j = 13$ to 20 eV with a step of 1 eV. The calculated $I(t)$ is insensitive to this step, provided that it is less than 1 eV. Figure 5(b) shows the integrated

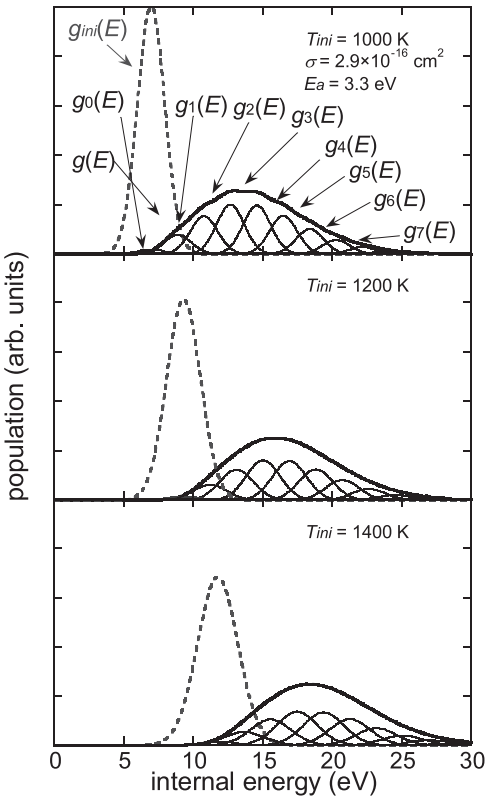

FIG. 4. Simulated energy distribution functions for different $T_{\rm ini}$ before photoabsorption, $g_{\rm ini}(E)$, and after photoabsorption, $g(E)$, when the F was 4.1 mJ/cm^2. Simulated energy distribution functions for various n-photon processes, $g_n(E)$; n = 0–10 are also shown. For $n \geqslant 8$, $g_n(E)$ is barely visible in this figure because of its low amplitude.

intensity for each energy component for the demonstration of the presence of the energy window. As mentioned in Sec. II, the neutral products could not be monitored up to a few tens of μs for t; thus, the components for $E \geqslant 19$ eV were undetectable in the experiments. Conversely, the ions with low E, e.g., the 13-eV component, do not significantly contribute to the shape of $I(t)$ in this time range because of their low intensity. This profile is mainly ascribed to a sharp change in the $k(E)$ values, and is not sensitive to the variation of $g(E)$. For the $ZnPc^-$ ions studied in our ring configuration, the decays of the photoexcited ions in the energy window of 14 to 18 eV were selectively detected in the experiments. Variations of $g(E)$ occurring outside the window do not influence the observations.

Figure 6(a) shows the $T_{\rm ini}$ dependence of the simulated $I(t)$ where all $I(t)$ were normalized to intensities at $t = 50$ μs. The simulated $I(t)$ curve decays faster for higher $T_{\rm ini}$. This trend agrees with the intuitive prediction that "the hotter decays faster." However, it should be noted that only the change in $g(E)$ inside the energy window is important. Figure 6(b) shows the simulated $g(E)$ for each $T_{\rm ini}$, and the energy window displayed as the bright area. The relative population of each $g(E_j)$ determines the shape of $I(t)$. It is noticeable that the distribution at higher $T_{\rm ini}$ has a large population at the large energy side in this area, leading to faster decay. In addition,

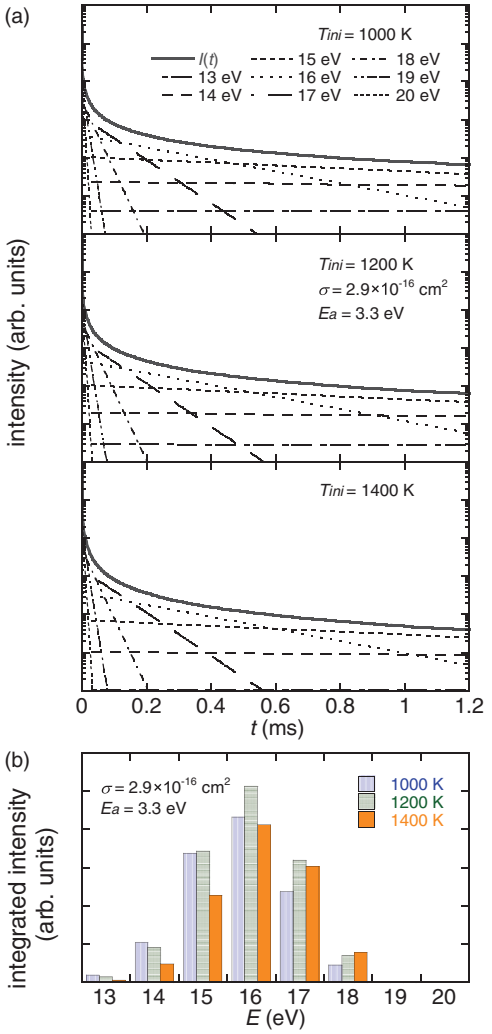

FIG. 5. (Color online) (a) Semilog plots of simulated decay profiles at the same $T_{\rm ini}$ as Fig. 4 for the various internal energies from 13 (the slowest) to 20 eV (the fastest) weighted by the distribution shown in Fig. 4 and the summed profiles, $I(t)$, over these components. F was 4.1 mJ/cm^2. (b) Bar graphs of the integrated intensity of each decay component (linear scale) over 0.05–1.05 ms at the $T_{\rm ini}$ shown in (a).

the separation of the simulated $I(t)$ curves becomes smaller for lower $T_{\rm ini}$, which is consistent with our observation if the ions are not very hot.

2. *F dependence of I(t)*

The F dependence of the simulated $I(t)$ for $T_{\rm ini} = 1300$ K displayed in Fig. 7(a) well reproduces the experimental results [Fig. 2(b)]. It is explained again in terms of $g(E)$ lying in the window shown in Fig. 7(b). As in the case of the $T_{\rm ini}$ dependence of the simulated $I(t)$, the distribution at higher F has a large population in the large energy side. We comment that such F dependence does not exist naturally under extremely low F conditions where the one-photon absorption condition is satisfied, although the detection of the photoinduced neutral products under such condition is experimentally difficult.

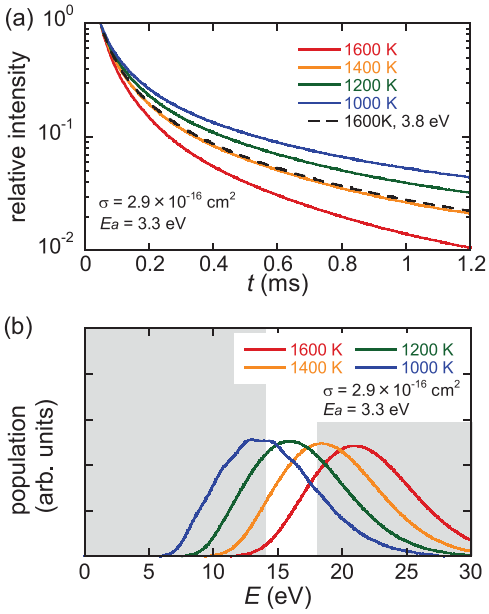

FIG. 6. (Color online) (a) Semilog plot of simulated $I(t)$. Bold lines: for $T_{\rm ini}$ from 1000 (top) to 1600 K (bottom) when F was 4.1 mJ/cm^2. Dashed line: reference $I(t)$ for $T_{\rm ini} = 1600$ K and for $E_a = 3.8$ eV. Note that the vertical scale is enlarged compared to Fig. 5. All curves are normalized to the intensity at $t = 50\,\mu$s. (b) Simulated $g(E)$ (linear scale) for different $T_{\rm ini}$ from 1000 (left) to 1600 K (right). The bright area represents the detectable energy range.

3. *F dependence of the total yield ($I_{\rm sum}$)*

To understand the storage time dependence of the $I_{\rm sum}$-F plots [Fig. 2(c)], we simulate the $T_{\rm ini}$ dependence. The simulated curves well reproduce the experimental results including the "saturation" behavior. The curve reaches maximum and then begins to decline, suggesting that the flat-topped plots for 20 and 80 ms storage times in Fig. 2(c) are a sign of the drop at the even higher F. The distribution of $g(E)$ in the energy window also plays a key role in this behavior. Considering the case for 1600 K, for instance, the F dependence of $g_1(E)$, $g_2(E)$, and $g_3(E)$ is displayed in Fig. 8(b). The one-photon component $g_1(E)$ is located in the middle of the window where the contribution to the $I_{\rm sum}$ is most effective. The $g_2(E)$ curve lies in the less effective high-energy side, and the $g_3(E)$ lies almost outside the window. Since the areal intensity of each curve is determined by Eq. (4), it shows a decrease at large σD, or high F, leading to a decrease in $I_{\rm sum}$.

For $T_{\rm ini}$ lower than 1600 K, $g_n(E)$ with larger n will contribute to the total yield since $g_{\rm ini}(E)$ for such $T_{\rm ini}$ shifts to lower E. Accordingly, the increase in $I_{\rm sum}$ in the low-F region becomes steeper and the peak shifts to the higher-F side.

Summarizing, the model simulation well reproduces the general trends of the experimental results and suggests that the detachment behavior is governed by $g(E)$ located in the energy window.

C. Parameter dependence of the simulation

The simulation tells us that the $I(t)$ curves strongly change depending on $T_{\rm ini}$ at the *high*-$T_{\rm ini}$ region, whereas it becomes less sensitive at lower (or *moderately high*) $T_{\rm ini}$. In contrast,

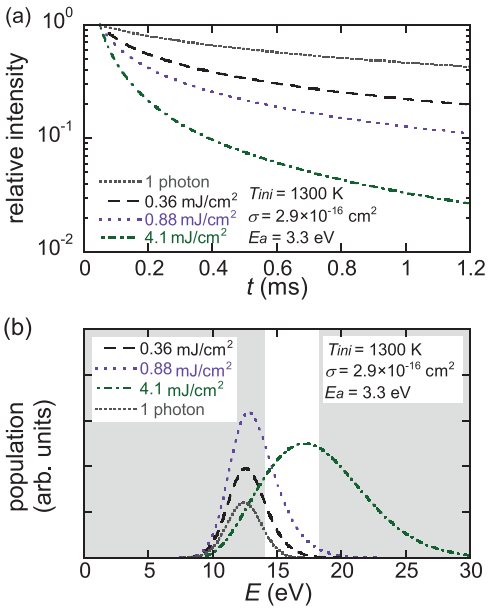

FIG. 7. (Color online) (a) Simulated $I(t)$ for four different F of 0.36 (top), 0.88 (middle), and 4.1 mJ/cm^2 (bottom). All curves are normalized to the intensity at $t = 50$ μs. The case for one-photon absorption (top) is added. (b) Simulated $g(E)$ for the same condition as (a).

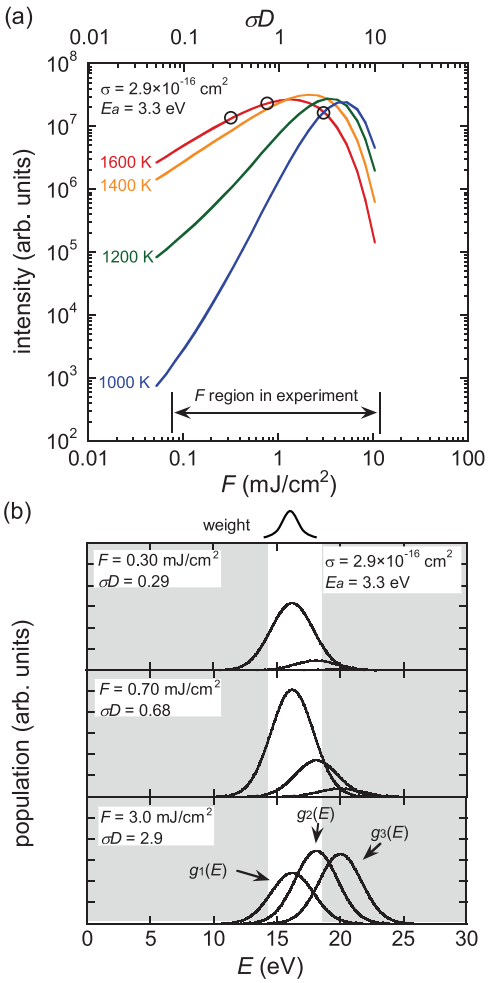

FIG. 8. (Color online) (a) Log-log plots of the simulated neutral yields depending on $T_{\rm ini}$ versus F and corresponding σD for σ of 2.9 $\times 10^{-16}$cm^2. The experimental F region is indicated in the right bottom corner of this figure. (b) Population of $g_1(E)$, $g_2(E)$, and $g_3(E)$ for $T_{\rm ini}$ of 1600 K when F is 0.30 (top), 0.70 (middle), and 3.0 mJ/cm^2 (bottom). The corresponding $I_{\rm sum}$ values for these F values are shown as circles in (a). The amplitude of the distributions is directly comparable for different F. The bright area represents the energy window, and a curve drawn on the top of this figure illustrates the weight function for the yield, as shown in Fig. 5(b).

the F dependence of the $I_{\rm sum}$ curves is sensitive to $T_{\rm ini}$ at *moderately high* $T_{\rm ini}$, whereas these are similar at the *high*-$T_{\rm ini}$ region. Thus, the suitable procedure to estimate $T_{\rm ini}$ from the experimental results is different for a *hot* target and *moderately hot* target. From the simulation we speculate that the boundary of *high* and *moderately high* $T_{\rm ini}$ is approximately 1400 K [see Figs. 6(a) and 8(a)].

It is also emphasized that the present simulation relies on the input parameters of the photoabsorption cross section (σ), electron affinity (E_a), heat capacity, and electron attachment cross section, although accurate values for these molecular properties are not available. In the following discussion, we examine how the evaluated $T_{\rm ini}$ varies depending on these parameters. The argument concerns the uncertainty of the evaluated $T_{\rm ini}$; in addition, it allows extending the $T_{\rm ini}$ evaluation procedure to other molecular systems. In the present study, although the experimental uncertainty is another critical factor, we focus on the parameter dependence of $T_{\rm ini}$.

The σ value was needed for the calculation of $g(E)$ through Eq. (3). Since $g(E)$ is given as a function of σD, the $I(t)$ profile and $I_{\rm sum}$ are affected by the choice of σ. The adopted value of σ in the simulation is 2.9 $\times$ 10^{-16} cm^2, measured in solution at room temperature. For neutral ZnPc, the absorption spectrum of a hot molecule in the gas phase (830 K) [28] is reported and the cross section at approximately 670 nm is 50% lower than that obtained in the solution at room temperature. Considering that a similar reduction might occur at the ZnPc$^-$ ion, we examined the variation of σ from 1.0 to 3.0 $\times 10^{-16}$ cm^2.

The exponential dependence of $k(E)$ on E (see Fig. 3) suggests the need for accurate E_a values for simulating the delayed detachment behavior, as demonstrated in the cases of clusters [29]. Theoretical values of E_a are 3.3 and 3.8 eV, depending on the calculation level [27]. We examined $T_{\rm ini}$ as a function of E_a ranging from 3.1 to 4.0 eV to cover the reported range of values. Roughly, the increase in E_a by $+0.1$ eV reduces the $k(E)$ by a third at $E = 10$ eV and by half at 20 eV. The $T_{\rm ini}$ values are less sensitive to the other parameters used in the calculation of $k(E)$. For example, a 10% increase in the heat capacity and the electron attachment cross section leads to a change in $T_{\rm ini}$ by approximately +50, and -10 K, respectively. For comparison, the $I(t)$ curve for a different value of E_a (3.8 eV) is shown in Fig. 6(a).

The $T_{\rm ini}$ variations as a function of σ and E_a estimated for the storage time of 80 ms by two independent schemes are shown in Fig. 9, where (a) shows the $T_{\rm ini}$ obtained from the $I(t)$ profile [Fig. 2(a)] and (b) shows that from the F dependence of $I_{\rm sum}$ [Fig. 2(c)]. The measurements corresponding to Figs. 9(a) and 9(b) should give the same $T_{\rm ini}$ value at the proper values of σ and E_a. Although this requirement would in turn restrict

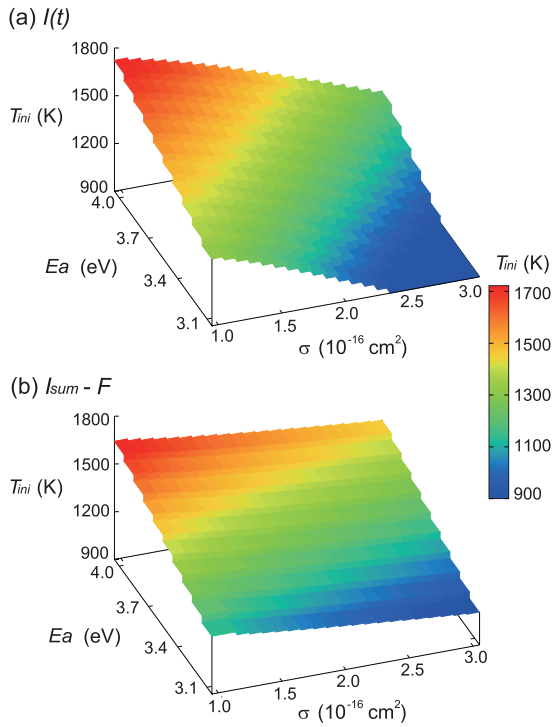

FIG. 9. (Color online) 3D plots displaying the evaluated $T_{\rm ini}$ as a function of σ and E_a from the analyses of (a) $I(t)$ profile and (b) $I_{\rm sum}$-F relation. The fitted experimental $I(t)$ and $I_{\rm sum}$ are for the storage time of 80 ms, as displayed in Figs. 2(a) and 2(c), respectively. The maximum evaluated $T_{\rm ini}$ is 1722 K through $I(t)$ for σ of 1.0×10^{-16} cm^2 and for E_a of 4.0 eV. The lower limit of $T_{\rm ini}$ in the present simulation is 900 K, as mentioned above. Fitting errors are ± 20 K for $I(t)$ and ± 10 K for $I_{\rm sum}$-F obtained after χ^2 minimization.

the values of σ and E_a, $T_{\rm ini}$ without these limits is shown in these figures, to clearly illustrate the dependence on σ and E_a. As can be seen, $T_{\rm ini}$ in Fig. 9(a) is more sensitive to the choice of parameters for this temperature range.

The 3D plots for other storage times show similar tendency, and considering all the plots together, in principle, we could determine the parameters more precisely. It should be noted that the uncertainty involved in the $T_{\rm ini}$ evaluation would be different because, as mentioned before, the $I(t)$ profile is less sensitive to the $T_{\rm ini}$ when it is relatively low and $I_{\rm sum}$-F relation is less sensitive to the $T_{\rm ini}$ when it is relatively high. In an extreme case, simultaneous constraint given by the two plots does not work. Thus, we suspend further analyses at the present stage.

IV. CONCLUSION

We have shown that the simulation well reproduces the experimental results of the laser-induced delayed detachment behavior, allowing one to properly understand the multiphoton-induced process. The importance of the energy window restriction imposed on the ion storage experiments was demonstrated. As for the $T_{\rm ini}$ determination in the present procedures, the ambiguity in σ and E_a values leads to large uncertainties.

For hot and large molecules, the multiphoton process readily occurred and was practically unavoidable in many cases. We have shown that the complexity associated with the multiphoton contributions decreased by imposing the selectivity by the "energy window." The analysis enables a rough estimation of the internal temperature, within the limit of accuracy of the molecular constants, for many other molecules.

ACKNOWLEDGMENTS

We thank Dr. Klavs Hansen (Gothenburg University) for the useful discussions. This work was supported by Grants-in Aid for Scientific Research (No. 19350015, No. 21200051, and No. 20750015). M.G. acknowledges support obtained from the MEXT program for Improving Graduate School Education. T.M. acknowledges support from the Matsuo foundation.

[1] E. E. B. Campbell and R. D. Levine, Annu. Rev. Phys. Chem. **51**, 65 (2000).
[2] B. A. Collings, A. H. Amrein, D. M. Rayner, and P. A. Hackett, J. Chem. Phys. **99**, 4174 (1993).
[3] D. Zajfman, O. Heber, L. Vejby-Christensen, I. Ben-Itzhak, M. Rappaport, R. Fishman, and M. Dahan, Phys. Rev. A **55**, R1577 (1997).
[4] H. T. Schmidt, H. Cederquist, J. Jensen, and A. Fardi, Nucl. Instrum. Methods Phys. Res., Sect. B **173**, 523 (2001).
[5] M. Lange, M. Froese, S. Menk, J. Varju, R. Bastert, K. Blaum, J. R. Crespo Lopez-Urrutia, F. Fellenberger, M. Grieser, R. von Hahn *et al.*, Rev. Sci. Instrum. **81**, 055105 (2010).
[6] S. P. Moller, Nucl. Instrum. Methods Phys. Res., Sect. A **394**, 281 (1997).
[7] T. Tanabe and K. Noda, Nucl. Instrum. Methods Phys. Res., Sect. A **496**, 233 (2003).
[8] S. Jinno, T. Takao, Y. Omata, A. Satou, H. Tanuma, T. Azuma, H. Shiromaru, K. Okuno, N. Kobayashi, and I. Watanabe, Nucl. Instrum. Methods Phys. Res., Sect. A **532**, 477 (2004).
[9] J. Bernard, G. Montagne, R. Brédy, B. Terpend-Ordaciére, A. Bourgey, M. Kerleroux, L. Chen, H. T. Schmidt, H. Cederquist, and S. Martin, Rev. Sci. Instrum. **79**, 075109 (2008).
[10] J. U. Andersen, L. N. Andersen, P. Hvelplund, A. Lapierre, S. P. Moller, S. B. Nielsen, U. V. Pedersen, and S. Tomita, Hyperfine Interact. **146/147**, 283 (2003).
[11] S. B. Nielsen, J. U. Andersen, P. Hvelplund, B. Liu, and S. Tomita, J. Phys. B **37**, R25 (2004).
[12] K. Hansen, J. U. Andersen, P. Hvelplund, S. P. Moller, U. V. Pedersen, and V. V. Petrunin, Phys. Rev. Lett. **87**, 123401 (2001).
[13] J. U. Andersen, E. Bonderup, and K. Hansen, J. Phys. B **35**, R1 (2002).
[14] Y. Toker, O. Aviv, M. Eritt, M. L. Rappaport, O. Heber, D. Schwalm, and D. Zajfman, Phys. Rev. A **76**, 053201 (2007).
[15] F. Lépine, B. Climen, M. Lebeault, and C. Bordas, Eur. Phys. J. D **55**, 627 (2009).
[16] J. Rajput, L. Lammich, and L. H. Andersen, Phys. Rev. Lett. **100**, 153001 (2008).
[17] A. Amrein, R. Simpson, and P. Hackett, J. Chem. Phys. **95**, 1781 (1991).

[18] A. E. K. Sundén, M. Goto, J. Matsumoto, H. Shiromaru, H. Tanuma, T. Azuma, J. U. Andersen, S. E. Canton, and K. Hansen, Phys. Rev. Lett. **103**, 143001 (2009).
[19] M. Goto, M. Togawa, S. Jinno, T. Takao, J. Matsumoto, H. Shiromaru, Y. Achiba, H. Tanuma, and T. Azuma, Chem. Phys. Lett. **460**, 46 (2008).
[20] Z. Liu, X. Zhang, Y. Zhang, and J. Jiang, Spectrochim. Acta, Part A **67**, 1232 (2007).
[21] Y. Zhao, E. de Beer, C. Xu, T. Taylor, and D. M. Neumark, J. Chem. Phys. **105**, 4905 (1996).
[22] J. U. Andersen, P. Hvelplund, S. B. Nielsen, U. V. Pedersen, and S. Tomita, Phys. Rev. A **65**, 053202 (2002).
[23] K. Mehlig, K. Hansen, M. Hedén, A. Lassesson, A. V. Bulgakov, and E. E. B. Campbell, J. Chem. Phys. **120**, 4281 (2004).
[24] L. H. Andersen, H. Bluhme, S. Boyé, T. J. D. Jorgensen, H. Krogh, I. B. Nielsen, S. B. Nielsen, and A. Svendsen, Phys. Chem. Chem. Phys. **6**, 2617 (2004).
[25] T. Tanabe, M. Saito, and K. Noda, Eur. Phys. J. D **62**, 191 (2011).
[26] J. Mack and M. J. Stillman, J. Am. Chem. Soc. **116**, 1292 (1994).
[27] T. G. Gantchev, J. E. van Lier, and D. J. Hunting, Radiat. Phys. Chem. **72**, 367 (2005).
[28] L. Edwards and M. Gouterman, J. Mol. Spectrosc. **33**, 292 (1970).
[29] M. W. Froese, F. Blaum, K. Fellenberger, M. Grieser, M. Lange, F. Laux, S. Menk, D. A. Orlov, R. Repnow, T. Sieber, Y. Toker *et al*., Phys. Rev. A **83**, 023202 (2011).